

Influence of MEA Catalytic Layer Location and Air Supply on Open-Cathode Direct Ethanol Fuel Cell Performance

D. A. Moreno-Jiménez, D.E. Pacheco-Catalán, L.C. Ordóñez*

Unidad de Energía Renovable. Centro de Investigación Científica de Yucatán, A.C. C43 No. 130 Col. Chuburná de Hidalgo, Mérida, Yucatán, 97200. Mexico.

*E-mail: lcol@cicy.mx

Received: 6 July 2015 / Accepted: 4 September 2015 / Published: 30 September 2015

The influence of catalytic layer location on the performance of an open-cathode direct ethanol fuel cell (DEFC) was investigated using three different manufacturing methods for the membrane electrode assembly (MEA). The catalyst loading on both anode and cathode electrodes was 1 mgPtcm^{-2} . In MEA1, the anodic and cathodic catalyst layers (CL) were deposited directly onto the Nafion® membrane surface. MEA2 consisted of two CLs: an inner CL placed on the membrane surface and an outer CL located on the carbon cloth diffuser layer (DL). MEA3 was prepared using Pt-Black as the inner CL and PtRu/C or PtSn/C as the anode outer CL (MEA3a and MEA3b respectively). The combination of an inner and outer CL improved cell performance. Additionally, the incorporation of Pt black as the inner CL in MEA3 diminished ethanol crossover and improved DEFC performance through a significant decrease in mixed potential effects. Furthermore, we report the performance of an open-cathode DEFC using two operational approaches: air self breathing (ASB) and forced-air convection (FAC). The influence of air supply on DEFC performance was investigated via galvanostatic electrochemical impedance spectroscopy.

Keywords: DEFC, open-cathode, MEA preparation, CL location, ethanol crossover.

1. INTRODUCTION

Direct ethanol fuel cells (DEFCs) are attractive power source devices because alcohols can be easily handled, transported and stored using existing infrastructure. Furthermore, ethanol can be obtained with relative ease from biomass fermentation. It is not toxic like methanol and has a higher energy density [1]. Ethanol also presents lower membrane permeation rates in direct alcohol fuel cells, probably due to its larger molecular size [2]. Currently, in the context of highly portable power sources, DEFCs are proposed to power devices with low charge demands. However, it is necessary to

avoid energy outputs related to auxiliary systems such as air pumps or fuel supplies. As alternative, new bipolar plates with open-cathode architectures have been proposed, which can obtain oxygen directly from the air and avoid air pumps or pressurized tanks. There are two operational approaches for DEFCs using open cathodes [3, 4]: air self breathing (ASB), taking oxygen directly from air by diffusion, and forced-air convection (FAC), which uses fans to force the air into the cathode. The ASB approach is highly attractive, since parasitic loads from external devices are minimized. However, overall fuel cell performance is reduced due to slow oxygen diffusion [4]. On the other hand, the FAC approach gives higher cell performance through a reduction in mass transfer resistances [5, 6]. Nevertheless, the use of open-cathode architectures requires strict control of the air flow, since an excess could reduce the average temperature of the stack, causing a decrease in the electrochemical reaction rate [7]. The ionic conductivity of the electrolyte membrane has also been reported to decrease when relative humidity (RH) is below 100% [8, 9]. In open-cathode fuel cells, RH depends on ambient conditions and fuel cell temperature, which results in lower membrane conductivity than in a direct alcohol fuel cell with a controlled humidified oxygen supply. However, fuel cell portability tends to increase and numerous works include open-cathode designs [4, 7, 10-21].

The ratio between open area and electric contact is rather important. A high percentage of open area may cause increases in ohmic resistance [4]. Conversely, a low percentage of open area may promote oxygen mass transfer limitations [12]. For example, when the open area is increased from 52% to 92%, fuel cell performance decreases due to the higher ohmic loss caused by the longer electron pathways through the diffusion layer [9]. Hence, it is important to have an optimal ratio between open area and electrical contact, since this exerts a strong influence on the performance of open-cathode fuel cells. On the other hand, good performance of an open-cathode design requires an optimal design of the flow field channels and one of the most important aspects is the membrane electrode assembly (MEA). The improvement of MEA performance depends on the improvement of its individual components and the assembly process [22]. A lot of research has focused on different catalysts, the CL deposition method, operational conditions or different assembly methods to achieve higher MEA performance for ethanol fuel cells [10, 23-26], and it is clear that MEA design can improve performance in open-cathode operation.

MEA manufacturing must consider the optimal interaction between the reactants (liquid or gas), catalytic site and the electrolyte. Additionally, improvements could be achieved by lowering the electric resistance between the membrane, catalytic layer and diffusion layer and by decreasing the rate of ethanol crossover by changing the location of the catalytic layer, which essentially depends on the assembly process. There are two basic methods for the assembly process: a) deposition of the catalyst layer onto the DL, followed by hot pressing of the membrane between the electrodes; and b) deposition of the catalytic layer directly onto the membrane surface, followed by the addition and hot pressing of the DL. Membranes produced by this method are called catalyst-coated membranes (CCMs) [27].

Due to the importance of MEA manufacture and air supply on the global efficiency of open-cathode ethanol fuel cells, we constructed an open-cathode DEFC and studied the influence of catalytic layer location on its performance under two operational approaches: air self breathing and forced air convection. Three different methods for MEA preparation were investigated: a) Depositing catalyst layers (CL) directly onto the membrane surface; b) using two CLs, an inner layer placed on the

member surface and an outer CL located on the carbon cloth diffuser (DL); and c) using Pt-Black as the inner CL and PtRu/C or PtSn/C as the outer CL. Improved results were observed with the combination of an inner and outer CL. The approach for supplying air to the cathode also played an important role in mass transport limitations and DEFC performance.

2. EXPERIMENTAL

2.1. Materials

Nafion® 117 membrane (DuPont) was used in all experiments as a polymer electrolyte. We followed a three-step procedure to remove organic materials and activate the membrane. This consisted of boiling in 3% H₂O₂ solution for 45 minutes, boiling in 1 M H₂SO₄ for 45 minutes and washing in de-ionized water [28]. The commercial catalytic materials employed were Pt_{0.2}Ru_{0.1}/C HiSPEC™ 5000 (Alfa Aesar), Pt-Black (Alfa Aesar) and Carbon cloth EC-CC1 (ElectroChem Inc) for the DL. Graphite/polymer composite material was used for the anode and cathode plates of the single cell. Carbon-supported PtSn electrocatalyst with metallic loading of 50 wt% (Pt:Sn, 1:1, atomic ratio) was synthesized using sodium borohydride as the reduction agent and H₂PtCl₆ (Aldrich) and SnCl₃ (Aldrich) as metal precursors. Carbon Vulcan XC-72 was ultrasonically dispersed for 30 minutes in a three neck volumetric flask with 50/50 % v/v 2-propanol/de-ionized water solution. Appropriate amounts of Pt and Sn salts were then added to the dispersed carbon. The mixture was stirred for 3 h at room temperature, and then an appropriate amount of NaBH₄ solution was added drop by drop and stirred for 6 h. The obtained slurry was filtered, washed and dried in a vacuum oven at 80 °C overnight. Finally, the catalyst was thermally treated at 200 °C for 2 h in a nitrogen atmosphere.

2.2 Membrane electrode assembly preparation

The catalytic ink was prepared by mixing 33 µL of ionomer solution (5% w/w, Alfa Aesar) and 33 µL of 2-propanol per mg of Pt in the catalyst (Pt-black, PtRu/C or PtSn/C) for 30 minutes in an ultrasonic bath. Catalytic ink deposition was carried out by the brush painting method at different locations in the MEA. For comparisons, all MEAs had 9 cm² of electrode area with a catalyst loading of 1 mgPtcm⁻² in both anode and cathode electrodes. The membrane electrode assemblies (MEA) were prepared as follows (Fig. 1):

MEA1: Commercial PtRu/C catalyst was used in anode and cathode electrodes. The catalytic loading was 1 mgPtcm⁻². Catalytic ink was deposited directly on both sides of the membrane surface at 60 °C. A 9 cm² piece of carbon cloth was then placed over each catalytic layer and finally the MEA was assembled into the cell.

MEA2: Two CLs of PtRu/C were deposited on anode and cathode electrodes: an inner CL with a catalytic loading of 0.5 mgPtcm⁻² was coated directly onto the Nafion® membrane surface as with MEA-1. Next, an outer CL with a catalytic loading of 0.5 mgPtcm⁻² was coated onto the carbon cloth diffuser (DL). The total catalytic loading in the electrode was 1 mgPtcm⁻². Both anode and cathode

were prepared similarly. Finally, the membrane and electrodes were assembled by hot-pressing at 201 kgcm⁻² for 9 minutes at 120 °C.

MEA3: Two CLs were deposited on anode and cathode electrodes similarly to MEA2. An inner catalyst layer of Pt black with 0.5 mgPtc^m-² was coated directly onto the Nafion® membrane surface. A second catalyst layer was placed on the carbon cloth, referred to as the outer catalyst layer. In MEA3a, the cathode and anode outer CL contained PtRu/C catalysts. Meanwhile, in MEA3b the anodic outer CL consisted of PtSn/C catalyst. Finally, the electrodes were assembled by hot-pressing at 50 kgcm⁻² for 1 minute at 130 °C.

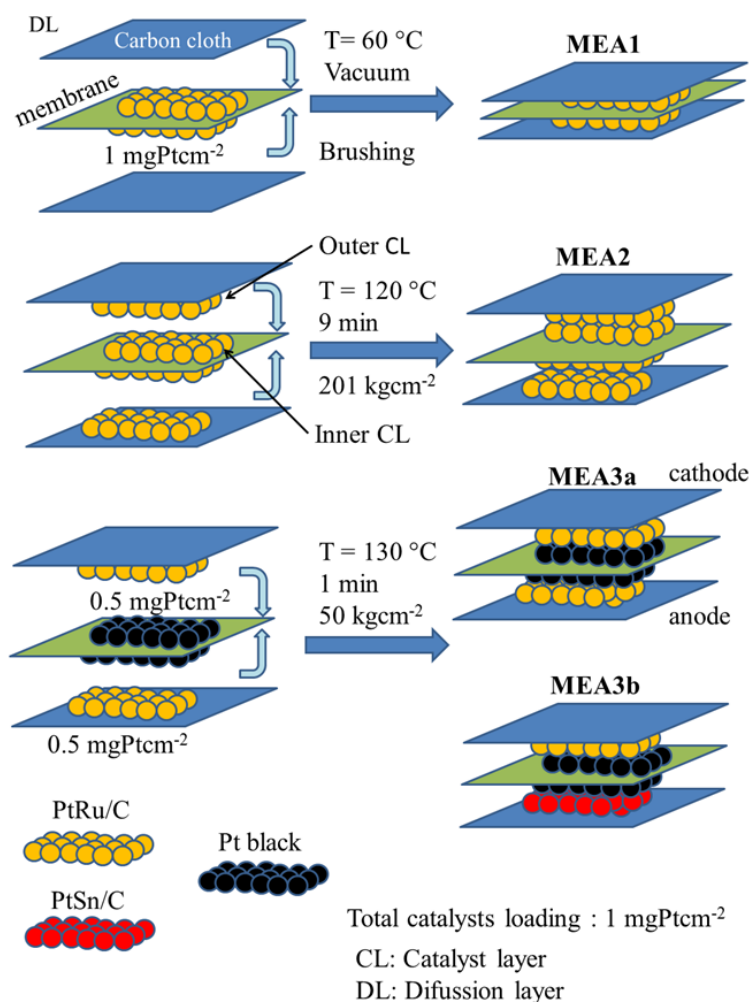


Figure 1. Catalytic layer location in different MEAs.

2.3 Open-cathode fuel cell design

The experiments were performed in an open-cathode DEFC designed in our laboratory. The anode flow field consists of a single-serpentine pattern (Fig. 2a). The cathode has a rhomboid array design that facilitates water removal and suitable air diffusion or convection into the cell. The cathode

side has an electrical surface contact area of 61%. In both electrodes the electrode active area is 9 cm². Figure 3 shows the complete open-cathode direct ethanol fuel cell.

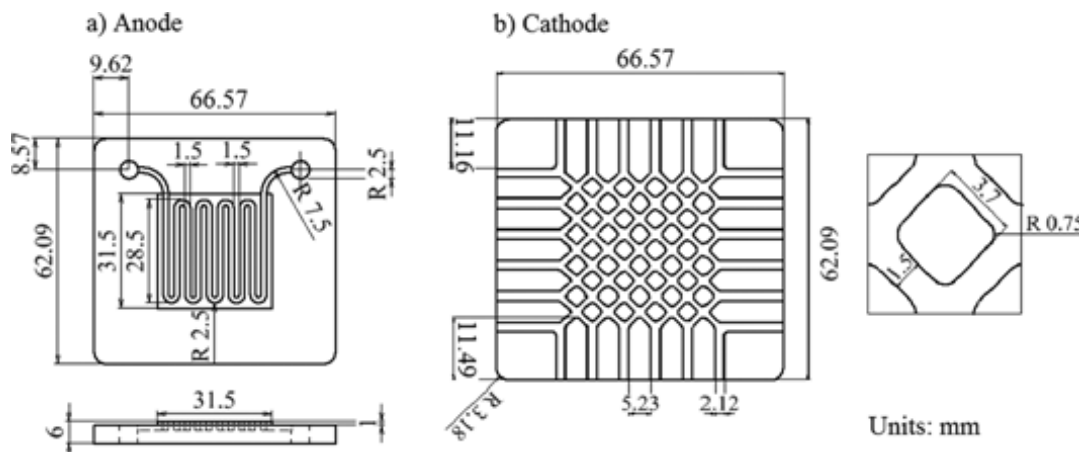


Figure 2. Open-cathode DEFC design: a) anode mono-polar plate, b) cathode mono-polar plate.

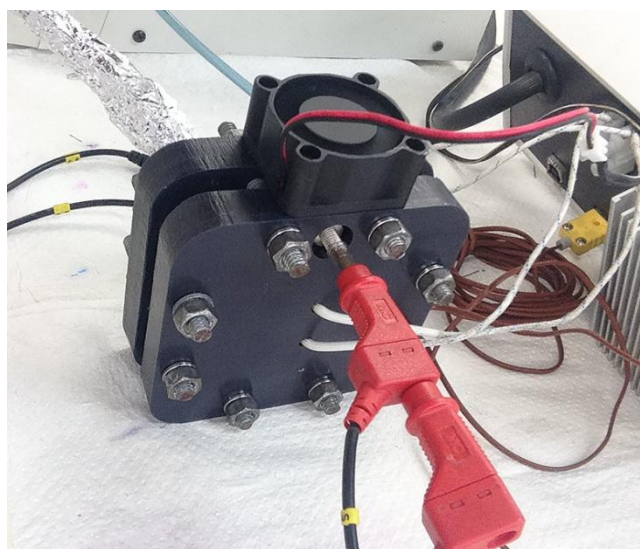


Figure 3. Open-cathode fuel cell operated under forced-air convection (FAC) air supply approach.

2.4 Cell performance test

The electrochemical measurements were performed with an AutoLab PGSTAT302 potentiostat/galvanostat. Before testing the cell, all MEAs were activated by heating the cell at to 60 °C and flowing 1.5 mLmin⁻¹ of deionized water through the anode side for 3 h to ensure suitable humidification of the membrane. Subsequently, a pulse potential of 100 mV was applied for 1800 s before fixing the voltage at 600 mV for 300s. This procedure was repeated twice. The polarization curves were registered using scan rates of 5 and 10 mVs⁻¹ at 25 and 60 °C. To assess the influence of the air supply approach on the global fuel cell performance, the cathode compartment was tested with

either air self breathing (ASB) or forced-air convection (FAC) operational modes. A galvanostatic electrochemical impedance spectroscopy (GEIS) test was carried out to evaluate the mass transport process and charge transfer resistance. GEIS spectra were obtained at a frequency range between 3 kHz and 0.1 Hz at a constant current that was very close to the limiting current in the mass transport zone of the polarization curve. 50 frequencies were recorded at a sinusoidal current amplitude of 6%. Additionally, a potentiostatic electrochemical impedance spectroscopy (PEIS) test was carried out to evaluate the ohmic resistance. PEIS spectra were obtained at a frequency range of 250 kHz - 0.01 Hz or 25 kHz - 0.1 Hz according to the response of each MEA. 50 frequencies were recorded at a sinusoidal voltage amplitude of 0.005 V at open circuit potential (OCP).

To carry out the crossover test, the open-cathode plate was replaced by one anode plate (Figure 2a) to obtain two single serpentine electrode compartments as in a conventional DEFC. This made it possible to flood the cathode compartment with deionized water to avoid the oxygen reduction reaction. Song *et al.* [29] suggest that in crossover tests the anode and cathode reactions are:



According to reactions (1) and (2), the hydrogen evolution reaction takes place on the anode side. Meanwhile, on the cathode side, the ethanol coming from the anode through the Nafion® membrane is electro-oxidized. In this configuration, the anode acts as a counter electrode and, at the same time, as a dynamic hydrogen reference electrode (DHRE). The cathode acts as a working electrode and electrochemically measures the amount of ethanol crossover in terms of current density. We evaluate the possible ethanol crossover decrease by placing a catalytic layer directly on the membrane. The ethanol oxidation at the cathode side (reaction 2) was followed using the cyclic voltammetry technique.

3. RESULTS AND DISCUSSION

3.1 MEA performance

Figure 4 shows the polarization curves registered for MEA1, MEA2 and MEA3a at 60 °C. Very close to the OCP can be observed similar potential values for MEA1 and MEA2, of 0.34 V and 0.36 V respectively. However, current and maximum power density increased with the use of two catalytic layers in MEA2, which could be attributed to lower ohmic resistance in this assembly caused by better contact between DL, CL and the membrane. This is because hot-pressing helps to reduce the resistance in the assembly in comparison with non-hot-pressed electrodes, as was observed in the comparison of EIS results (Table 1) between MEA1 and MEA2. MEA1 presented an ohmic resistance of 11.7 Ωcm^{-2} , compared to 2.61 Ωcm^{-2} for MEA2. In the case of MEA3b, which has an inner catalyst layer with Pt black, the OCP increased to 0.46 V and its maximum power density was almost twice that of MEA1: 0.72 mWcm^{-2} at 4.5 mAcm^{-2} vs. 0.8 mWcm^{-2} at 2.4 mAcm^{-2} . In this case, there is also

better contact between DL, CL and the membrane, which is expressed as the lowest ohmic resistance ($1.5 \Omega\text{cm}^{-2}$). The inner catalyst layer helps to reduce ethanol crossover, since Pt particles deposited onto the Nafion® membrane surface act as an ethanol barrier [26].

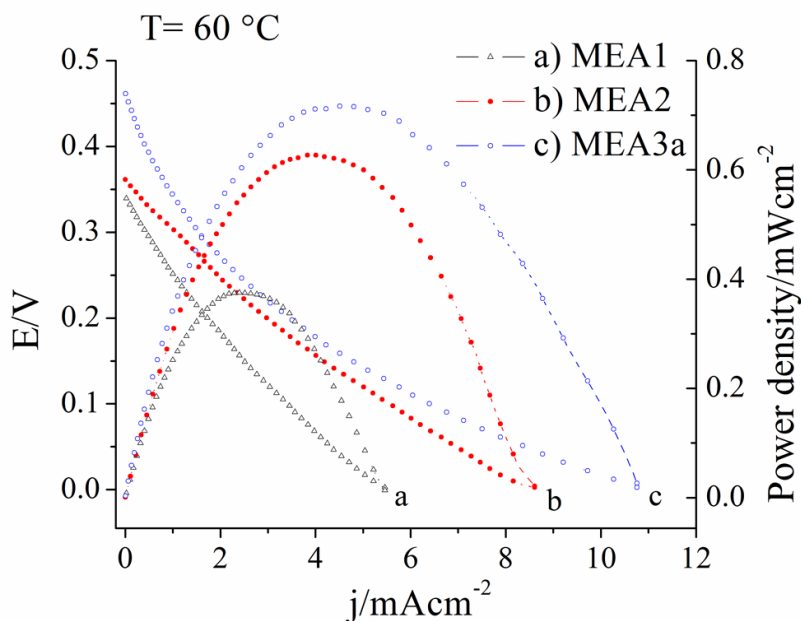


Figure 4. Polarization curves and power density for MEA1, MEA2 and MEA3a: ASB mode, scan rate of 10 mVs^{-1} . Fuel: 1 M ethanol solution at 1.5 mLmin^{-1} . $T = 60 \text{ }^\circ\text{C}$.

Table 1. Polarization results, ohmic resistances determined by potentiostatic EIS and ethanol crossover currents.

MEA	Ohmic resistance/ Ωcm^2	Maximum power density (mWcm^{-2})	Current density (mAcm^{-2})	OCP (V)
MEA1	11.7	0.38	2.4	0.34
MEA2	2.6	0.63	3.9	0.36
MEA3a	1.5	0.72	4.5	0.46

3.2 Ethanol crossover determination

Ethanol crossover was quantified electrochemically using the cyclic voltammetry (CV) technique, assuming that all ethanol that crossed from the anode to the cathode is converted into current at the cathode catalyst layer according to reaction 2. As such, the highest ethanol crossover corresponds to the highest current density produced by ethanol electro-oxidation [29]. Figure 5 shows the cyclic voltammograms for MEA1, MEA2 and MEA3b recorded at room temperature ($25 \text{ }^\circ\text{C}$). For MEA1 and MEA2, the ethanol oxidation peak appears at 0.84 V , while for MEA3 it appears at 0.94 V . This shift towards positive potentials means that ethanol electro-oxidation starts at a more positive potential than in MEA1 and MEA2. This was attributed to the catalysts contained in the inner catalyst

layer, since it has been reported that PtRu/C shows better activity than pure Pt catalysts [30]. It is known that Ru provides oxygen containing species that help to oxidize the adsorbed intermediates of the reaction [31]. On the other hand, the current density of each peak is related to the amount of ethanol permeated from the anode to the cathode. The currents for the peaks are MEA1 = 19.7 mAcm⁻², MEA2 = 17.9 mAcm⁻² and MEA3b = 12.5 mAcm⁻². It is clear that MEA3b shows the lowest current density related to permeation through the membrane, which means that the Pt black inner catalyst layer helps to mitigate crossover and improve the OCP through a decrease in mixed potential effects, similarly to what was observed by [32].

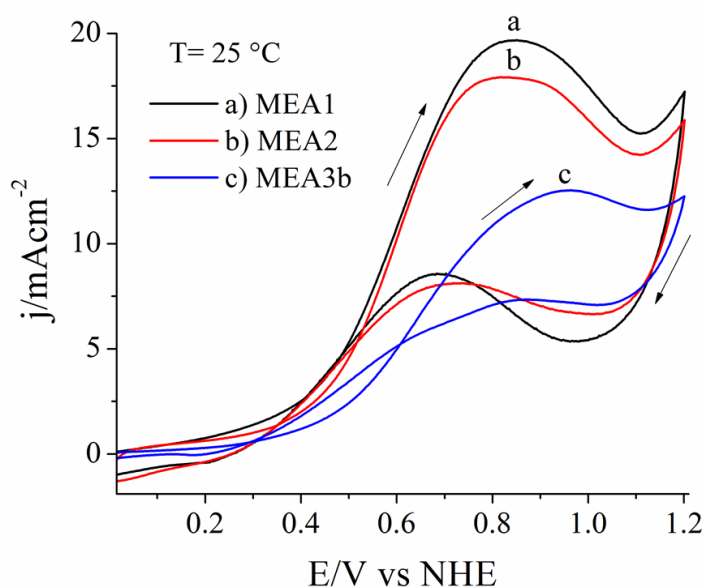


Figure 5. Ethanol crossover for MEA1, MEA2 and MEA3b at room temperature (25 °C): scan rate of 2 mVs⁻¹, 1.5 mLmin⁻¹ of 1 M ethanol solution in anode and flooded cathode.

3.3 Anode catalyst effect and air supply influence

PtSn/C and PtRu/C catalysts were deposited onto the outer layer in order to test their influence on MEA performance. The fact that PtSn/C presents better activity than PtRu/C for the ethanol oxidation reaction (EOR) has been widely studied [26, 33]. However, its influence as an outer catalyst layer in new MEA designs for open-cathode fuel cells is not yet clear. Figure 6 and Figure 7 show the polarization curves and power density of MEA3a and MEA3b at 25 °C and 60 °C respectively. In both cases, air self breathing (ASB) and forced-air convection (FAC) approaches were tested using a scan rate of 5 mVs⁻¹ and a feed of 1.5 mL/min of 1 M ethanol solution.

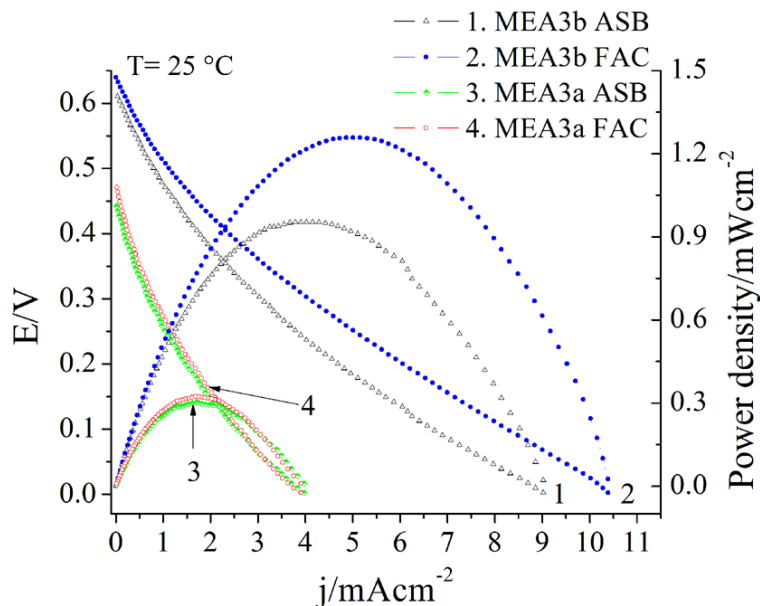


Figure 6. Polarization curves and power density for MEA3a and MEA3b. ASB and FAC operation modes. Scan rate of 10 mVs^{-1} . Fuel: 1M ethanol solution. $T = 25 \text{ }^\circ\text{C}$.

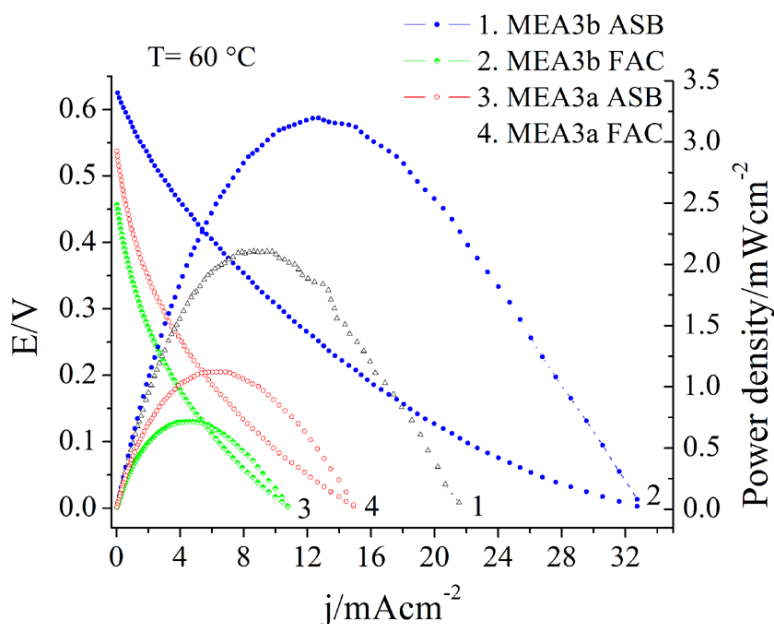


Figure 7. Polarization curves and power density for MEA3a and MEA3b. ASB and FAC operation modes. Scan rate of 10 mVs^{-1} . Fuel: 1M ethanol solution. $T = 60 \text{ }^\circ\text{C}$.

Table 2 presents the power densities of the MEAs in ASB and FAC mode at $25 \text{ }^\circ\text{C}$ and $60 \text{ }^\circ\text{C}$. MEA3b showed the highest peak power density (3.21 mWcm^{-2}) recorded at $60 \text{ }^\circ\text{C}$ in FAC mode. It can be seen that the OCP at $25 \text{ }^\circ\text{C}$ is higher with PtSn/C synthesized in our laboratory compared with commercial PtRu/C. At 25 and $60 \text{ }^\circ\text{C}$, the limiting current density and power density are higher using PtSn/C than PtRu/C. This represents an increase in the power density of around 68.8% in ASB mode and 74.6% in FAC mode at $25 \text{ }^\circ\text{C}$ for MEA3b with respect to MEA3a. Under air self breathing (ASB)

conditions, the water produced on the cathode side could limit oxygen access to the catalyst layer [34], which would mean that fuel cell performance is limited by an oxygen transport effect [35, 36].

Table 2. Power density of MEA3a and MEA3b at 25 °C and 60 °C.

MEAs	Power density under ASB mWcm ⁻²	Power density under FAC mWcm ⁻²	Temperature °C
MEA3a	0.30	0.32	25
MEA3b	0.96	1.26	25
MEA3a	0.72	1.13	60
MEA3b	2.10	3.21	60

MEA3b presented a reduction in peak power density between operation in ABS vs. FAC mode of around 23.8% at 25 °C and 34.5% at 60 °C (Figure 7). Considering the various advantages related to parasitic losses from external devices under ASB operation, our open-cathode fuel cell shows a relatively low decrease and could be operated with adequate performance in ASB mode, making portable applications more efficient.

The increase in fuel cell performance with the forced air supply approach is mostly related to an oxygen mass transport improvement as opposed to an ohmic resistance effect. Table 3 shows the ohmic resistances calculated by potentiostatic EIS and there is no significant variation between the two operational approaches, especially at 25 °C. Meanwhile, at 60 °C the ohmic resistance increased slightly, probably due to membrane dehydration caused by the airflow. However, in this case, forced-air convection mode helps to improve the oxygen diffusion and has the strongest influence on fuel cell performance.

Table 3. Potentiostatic EIS: ohmic resistance for MEA3a and MEA3b.

MEAs	Constant potential	Ohmic resistance	Ohmic resistance	Temperature °C
	(V) ASB/FAC	Ωcm ² ASB	Ωcm ² FAC	
MEA3a	0.46/0.52	1.6	1.6	25
MEA3b	0.63	1.3	1.3	25
MEA3a	0.46/0.57	1.5	1.9	60
MEA3b	0.63	1.08	1.5	60

Analysis of the galvanostatic impedance spectra was carried out to understand the effect of air supply, charge transfer resistance and oxygen mass transport on the performance of the fuel cell. All spectra were recorded in the mass transport zone of the polarization curves, close to the limiting current (Table 4), given that the mass transport effect is more significant in this zone and, in general for ASB designs, the performance of the fuel cell is limited by a lack of oxygen supply to the cathode [35]. Figure 8 shows the GEIS spectra for MEA3a and MEA3b under both operational approaches: ASB and FAC at 60 °C and feeding 1 M ethanol solution at 1.5 mL/min. MEA3a in ASB mode

presented the highest charge transfer resistance, while MEA3b in FAC mode presented the lowest. A similar trend was observed in both the EIS spectra (Figure 8) and the polarization curves (Figure 8 inset).

Table 4. Constant current values for galvanostatic EIS.

MEA	ASB Constant current (A)	FAC Constant current (A)	Temperature (°C)
MEA3a	0.07	0.11	60
MEA3b	0.19	0.27	60

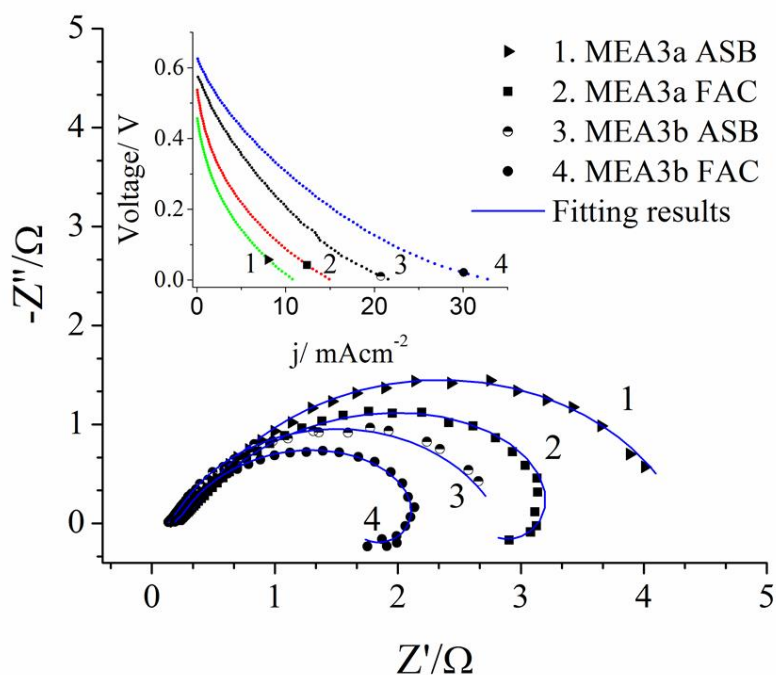


Figure 8. Galvanostatic EIS spectra for MEA3a and MEA3b in ASB and FAC mode at 60 °C, frequency range of 3 kHz to 0.1 Hz in mass transfer zone of polarization curve.

The GEIS spectra analysis was performed using the “fit and simulation” method based on the Boukamp model. Figure 9 shows the equivalent circuits proposed for the ASB and FAC operational approaches.

MEAs in ASB mode fit with a similar equivalent circuit for the anode and cathode. In this case, the interpretation of the circuit is $R_{ct1}/CPE_1 + R_{ohmic} + R_{ct2}/CPE_2$. The R_{ct1}/CPE_1 arrangement corresponds to a resistance-constant phase element in parallel on the anode side, and the same applies to R_{ct2}/CPE_2 on the cathode side. R_{ct1} and R_{ct2} are related to the charge transfer process of the anode and the cathode respectively. R_{ohmic} corresponds to the ohmic resistance that involves the ionic transfer resistance of the membrane and the electric transfer resistance of the fuel cell components. The CPE

element could represent a pure resistance when the exponent $N = 0$, a Warburg element when $N = 0.5$, a pure capacitor when $N = 1$ or an inductance when $N = -1$ [37, 38]. Usually, for values in a range from 0.9 to 0.99, the CPE is related to a non-ideal double layer capacitance attributed to a non-homogenous surface of the electrodes [38]. In general, for values of $N = 1 - n$, where $0 < n \leq 0.2$, the CPE corresponds to a capacitance distortion due to electrode surface roughness or distribution/accumulation of charge carriers. For $N = 0.5 \pm n$, where $0 < n \leq 0.1$, the CPE represents a diffusion effect with a deviation from Fick's second law. For $N < 0$, the CPE is related to inductive energy accumulation [37]. For each whole value of N , the coefficient Y_0 has a physical meaning (see Table 5). In this case, CPE_1 represents a Warburg element and CPE_2 corresponds to a pure capacitor (Table 6).

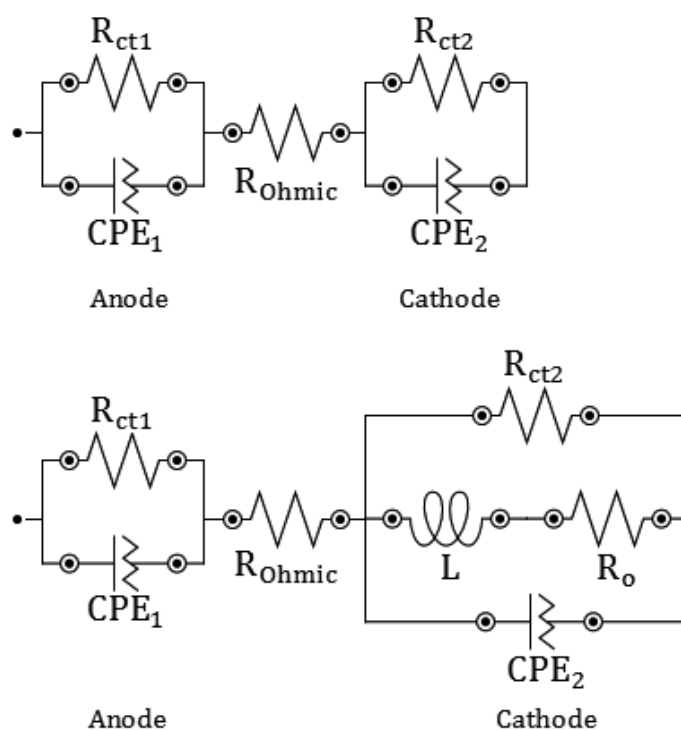


Figure 9. Equivalent circuits for MEA3a and MEA3b: a) ASB mode, b) FAC mode.

Table 5. Physical meaning of coefficient Y_0 [37].

N	CPE designation	Y_0 meaning	Units
1	Capacitance	C	$F = \Omega^{-1}s$
0	Resistance	R-1	Ω^{-1}
-1	Inductance	L-1	$H-1 = \Omega^{-1}s^{-1}$
0.5	Warburg element	$\sigma-1$	$\Omega s^{-1/2}$

CPE impedance; $Z_{CPE}(\omega) = Y_0^{-1} (j\omega)^{-N}$

Table 6. Values of equivalent circuit elements for MEA3a and MEA3b in ASB operation mode.

MEA	R_{ct1} (Ω)	CPE1 $\Omega s^{-1/2}/N$	R_{ohmic} (Ω)	R_{ct2} (Ω)	CPE2 F/N	Chi-squared X^2
MEA3a	0.29	174E-3/0.55	0.161	3.88	55.6E-3/0.80	0.02
MEA3b	0.05	151E-3/0.67	0.129	2.66	64.5E-3/0.79	0.14

Similarly, for the MEAs under FAC, the equivalent circuit has the following interpretation: $R_{ct1}/CPE1$ corresponds to the charge transfer process of the anode side, where CPE_1 corresponds to the double layer capacitance (non-ideal) attributed to the electrode- electrolyte interphase [39]. R_{ohmic} is related to the membrane resistance and all components of the fuel cell. R_{ct2} is related to the charge transfer process of the cathode. CPE_2 corresponds to a pure capacitor representing the double layer at the cathode. In this case, the series combination of $L + R_o$, inductance – resistance, fits the inductive loop behavior at low frequencies (Figure 7). This behavior has been observed in previous EIS studies and is related to oxygen mass transport, since this loop is often masked by oxygen diffusion limitations [39]. In this study, based on the simulation, it was observed that largest value was the resistance R_o , while the inductive loop tends to disappear. In other words, R_o can be attributed to the oxygen diffusion resistance.

Table 7. Values of equivalent circuit elements for MEA3a and MEA3b in FAC operation mode.

MEA	R_{ct1} (Ω)	CPE1 F/N	R_{ohmic} (Ω)	R_{ct2} (Ω)	CPE2 F/N	L (H)	R_o (Ω)	Chi-squared X^2
MEA3a	0.047	10.6E-3/0.947	0.215	3.65	46.1E-3/0.713	6.32	7.8	0.02
MEA3b	0.028	11E-3/0.996	0.185	2.25	52.2E-3/0.752	3.60	4	0.01

The values obtained from the fit and simulation method for MEA3a and MEA3b are presented in Table 6 and Table 7 respectively for ASB and FAC operation modes. In ASB mode, the charge transfer process of the anode in MEA3b presents lower R_{ct1} than MEA3a (Table 6). This means that the outer catalyst layer of PtSn/C promotes a faster reaction kinetic for ethanol electro-oxidation than PtRu/C. CPE_1 has N exponent values close to 0.5, which indicates Warburg element behavior related to a diffusion process. CPE_2 presented a capacitance or pseudo-capacitance effect with values of the N exponent near to positive units. Furthermore, MEA3b presents a lower R_{ohmic} than MEA3a, indicating better contact between the membrane, catalyst layers and DL. For MEA3b, R_{ohmic} was 0.129 or 1.616 Ωcm^2 in ASB and 0.85 Ω or 1.665 Ωcm^2 in FAC mode. Meanwhile, for MEA3a R_{ohmic} was 0.161 or 1.449 Ωcm^2 in ASB and 0.215 Ω or 1.9 Ωcm^2 in FAC mode. This slight increase in R_{ohmic} produced in FAC mode is less significant than the effect of the decrease in the charge transfer resistance (R_{ct}) on fuel cell performance. In FAC mode, an inductive loop was observed at low frequencies in both

MEAs, which indicates a decrease in the oxygen diffusion limitation. In this way, MEA3b showed the lowest resistance to the oxygen diffusion R_o value (4Ω or $36 \Omega\text{cm}^2$) in comparison to the R_o (7.80Ω or $70.2 \Omega\text{cm}^2$) value found in MEA3a. Also, R_{ct2} was observed to decrease with the use of forced-air convection, probably due to the increase in the limiting current of the cell since the oxygen mass transport problems are minimized. Under both operational approaches, MEA3b showed a lower R_{ct} than MEA3a. In fact, the larger the diameter of the semicircle in the impedance spectra, the lower the power density in the polarization curve [40], as can be clearly seen in Figure 8.

4. CONCLUSIONS

The influence of catalytic layer location and air supply on performance was determined by testing three different MEA preparation methods and two open-cathode operational approaches. The ohmic resistance was observed to be affected by the assembly method in MEA1 and MEA2, since improved contact between the DL, CL and the membrane gives lower ohmic resistances. In this case, the use of two catalytic layers, an inner one directly deposited onto the Nafion® membrane surface and another outer catalyst layer deposited onto the DL, helps to improve the contact resistance, generating higher power and current densities. Additionally, the use of an inner catalyst layer containing unsupported Pt black shows a significant increase in the OCP due to a decrease in the ethanol crossover rate, since the Pt black particles act as a reactive ethanol filter. The use of PtSn/C on the anode outer catalyst layer presented a faster reaction kinetic than PtRu/C, as determined by GEIS analysis of the R_{ct1} values in both MEAs. The increase in current and power density is mainly related to a decrease in the resistance to charge transfer than a variation of ohmic resistance. Air supply to the cathode also has a significant impact on cell performance. The forced-air convection operation mode helps to improve oxygen transport, which causes higher power and current density.

ACKNOWLEDGEMENTS

The authors acknowledge the financial support received from CONACYT-181106 and hydrogen thematic network (252003). D. Alejandro Moreno thanks CONACYT for grant No. 345947. The authors express their gratitude to Saúl Alexis Heredia for his collaboration on the DEFC design and manufacturing and Gustavo Martínez for technical support in the laboratory.

References

1. P. Ekdharmasuit, A. Therdthianwong, S. Therdthianwong, *Fuel*, 113 (2013) 69.
2. S. Song, P. Tsiakaras, *Appl Catal B-Environ*, 63 (2006) 187.
3. W. Liu, Y. Xie, J. Liu, X. Jie, J. Gu, Z. Zou, *Int J Hydrogen Energ*, 37 (2012) 4673.
4. N. Bussayajarn, H. Ming, K.K. Hoong, W.Y. Ming Stephen, C.S. Hwa, *Int J Hydrogen Energ*, 34 (2009) 7761.
5. K.S. Dhathathreyan, N. Rajalakshmi, K. Jayakumar, S. Pandian, *International Journal of Electrochemistry*, 2012 (2012) 7.
6. Q. Wang, G. Wang, X. Lu, Ch. Chen, Z. Li, G. Sun, *Int J Electrochem Sci*, 10 (2015) 2939.

7. F. Barreras, A.M. López, A. Lozano, J.E. Barranco, *Int J Hydrogen Energ*, 36 (2011) 7612.
8. H. R. Corti, E. R. González, *Direct Alcohol Fuel Cells*, Springer, Netherlands (2013).
9. S. U. Jeong, E.A. Cho, H.J. Kim, T.H. Lim, I.H. Oh, S.H. Kim, *J Power Sources*, 158 (2006) 348.
10. R.I. Jafri, S. Ramaprabhu, *Int J Hydrogen Energ*, 35 (2010) 1339.
11. S. Giddey, S.P.S. Badwal, D. Fini, *Int J Hydrogen Energ*, 37 (2012) 11431.
12. T. Hottinen, M. Mikkola, P. Lund, *J Power Sources*, 129 (2004) 68.
13. K. Y. Song, H.K. Lee, H.T. Kim, *Electrochim Acta*, 53 (2007) 637.
14. J. G. Liu, T.S. Zhao, R. Chen, C.W. Wong, *Electrochem Commun*, 7 (2005) 288.
15. T. V. Reshetenko, H.T. Kim, H.J. Kweon, *J Power Sources*, 171 (2007) 433.
16. W. Yuan, Y. Tang, X. Yang, B. Liu, Z. Wan, *Int J Hydrogen Energ*, 37 (2012) 9298.
17. L. Sun, C. Liu, J. Liang, X. Zhu, T. Cui, *J Power Sources*, 196 (2011) 7533.
18. S. H. Kim, H.Y. Cha, C.M. Miesse, J.H. Jang, Y.S. Oh, S.W. Cha, *Int J Hydrogen Energ*, 34 (2009) 459.
19. G. B. Jung, K.F. Lo, A. Su, F.B. Weng, C.H. Tu, T.F. Yang, S.H. Chan, *Int J Hydrogen Energ*, 33 (2008) 2980.
20. K. I. Lee, S.W. Lee, M.S. Park, C.N. Chu, *Int J Hydrogen Energ*, 35 (2010) 11844.
21. W. Yuan, Y. Tang, Z. Wan, M. Pan, *Int J Hydrogen Energ*, 36 (2011) 2237.
22. B. Wu, B. Li, W. Liu, J. Liu, M. Zhao, Y. Yao, J. Gu, Z. Zou, *Int J Hydrogen Energ*, 38 (2013) 10978.
23. Z. Wei, S. Wang, B. Yi, J. Liu, L. Chen, W. Zhou, W. Li, Q. Xin, *J Power Sources*, 106 (2002) 364.
24. H. Pramanik, A.A. Wragg, S. Basu, *J Appl Electrochem*, 38 (2008) 1321.
25. S. K. Biswas, P. Sambu, S. Basu, *Asia Pac J Chem Eng*, 4 (2009) 3.
26. C. H. Wan, C.L. Chen, *Int J Hydrogen Energ*, 34 (2009) 9515.
27. V. Mehta, J.S. Cooper, *J Power Sources*, 114 (2003) 32.
28. Y. Sone, P. Ekdunge, D. Simonsson, *J Electrochem Soc*, 143 (1996) 1254.
29. S. Song, G. Wang, W. Zhou, X. Zhao, G. Sun, Q. Xin, S. Kontou, P. Tsiakaras, *J Power Sources*, 140 (2005) 103.
30. Z. Liu, X.Y. Ling, X. Su, J.Y. Lee, L.M. Gan, *J Power Sources*, 149 (2005) 1.
31. Y. C. Park, D.H. Peck, S.K. Dong, S.K. Kim, S. Lim, D.H. Jung, J.H. Jang, D.Y. Lee, *Int J Hydrogen Energ*, 36 (2011) 1853.
32. C.H. Lin, C.H. Wan, W. Wu, *Int J Electrochem Sci*, 8 (2013) 8236.
33. S. Q. Song, W.J. Zhou, Z.H. Zhou, L.H. Jiang, G.Q. Sun, Q. Xin, V. Leontidis, S. Kontou, P. Tsiakaras, *Int J Hydrogen Energ*, 30 (2005) 995.
34. D. Kim, E.A. Cho, S.A. Hong, I.H. Oh, H.Y. Ha, *J Power Sources*, 130 (2004) 172.
35. Z.R. Willamson, D. Chun, K. Kwon, T. Lee, C.W. Squibb, D. Kim, *Appl Therm Eng*, 56 (2013) 54.
36. Y. Tabe, S.K. Park, K. Kikuta, T. Chikahisa, Y. Hishinuma, *J Power Sources*, 162 (2006) 58.
37. X. Z. Yuan, C. Song, H. Wang, J. Zhang, *Electrochemical impedance spectroscopy in PEM fuel cells Fundamentals and Applications*, Springer-Verlag, London, (2010).
38. E. Barsoukov, Jr. Macdonald, *Impedance Spectroscopy Theory, Experiment, and Applications*, second edition, John Wiley & Sons, Inc., Hoboken, New Jersey, (2005).
39. C. Y. Du, T.S. Zhao, W.W. Yang, *Electrochim Acta*, 52 (2007) 5266.
40. T. V. Reshetenko, H.T. Kim, H. Lee, M. Jang, H.J. Kweon, *J Power Sources*, 160 (2006) 925.